Journal of
Mechanical
Science and
Technology

Journal of Mechanical Science and Technology 21 (2007) 2178~2187

An investigation of local heat transfer characteristics in a ventilated disc brake with helically fluted surfaces

Sung Bong Park[1], Kwan Soo Lee[1] and Dae Hee Lee[2,*]

[1]*School of Mechanical Engineering, Han Yang University, Haengdang-Dong 17, Seoul 133-791, Korea*
[2]*School of Mechanical and Automotive Engineering, Inje Engineering Institute, Inje University, 607 Obang-Dong, Gimhae, Gyeongnam 621-749, Korea*

(Manuscript Received April 6, 2007; Revised June 20, 2007; Accepted June 20, 2007)

Abstract

Local Nusselt numbers in the cooling flow passage of the automobile disc brake with helically fluted surfaces are presented. The flat surface in the flow passage is modified to the helically fluted surface for the purpose of enhancing the heat transfer rate, thereby reducing the thermal stress and deformation in the disc brake. Thermochromic liquid crystals and shroud-transient technique are used to measure spatially-resolved surface temperature distributions, which are used to deduce local Nusselt numbers. The Reynolds number Re ranges from 30,000 to 70,000, the helix angle θ is fixed at 45° and the dimensionless streamwise distance z/d ranges from 1.5 to 4.5. The results show that in general, local Nusselt numbers monotonically decrease with a distance away from both windward and leeward crests of the helical flute and reach a minimum value near its valley for all Re's and z/d's tested. The local Nusselt numbers on the helically fluted grooves are maximum 51.6 to 93.7% higher than values measured on the flat surface. The heat transfer enhancement magnitudes become more pronounced with smaller Re and z/d. The largest enhancement occurs at the windward side of the helical flute at z/d = 1.5 and Re = 30,000. It is also found that at Re = 30,000 the average Nusselt numbers on the helically fluted surface are maximum 37 % higher than those on the flat surface. The numerical results show that with 10 braking cycles, the temperatures with helically fluted surface are maximum 44.3 %, 36.8 %, and 36.6 % lower than those with the flat surface in the inlet, the center, and the outlet, respectively.

Keywords: Disc brake; Local Nusselt number; Liquid crystal; Helically fluted surface

1. Introduction

The number of cars on the streets continues to increase and more accidents occur due to brake failure. And as highway speed limits have gradually increased, braking systems must operate under more adverse conditions. Day and Ashi [1] studied how to dramatically shorten the braking distance under such conditions. The surface of a brake disc plate can reach temperatures as high as 800°C, resulting in material property changes. When cooling occurs, the carbon steel changes from a pearlite to a martensite structure, which has larger carbon structures. This change causes the volume of the disc plate to increase by 4%, introducing disc thickness variation (DTV), defacement, thermal cracks, and judder. These harmful effects create squeals and vibration, and eventually shorten the life span of the braking system or result in a sudden failure. As the brake assimilates the kinetic energy of a vehicle through the contact frictional force between two objects, the work of the frictional force changes to heat energy, causing a temperature rise in the contact parts. Therefore, the heat emission ability of a braking system influences the efficiency and life of the brakes. Since the temperature distribution is more important than the loading stress, the shapes of a brake disc and pad are designed to provide suitable cooling.

The braking ability of a vehicle can be lost when

*Corresponding author. Tel.: +82 55 320 3185, Fax.: +82 55 324 1723
E-mail address: mechdhl@inje.ac.kr

recursive braking is applied over many hours of vehicle operation due to the frictional heat generated at the point of contact between the disc and pad. If the heat is not released to the ambient air properly, the performance of the brake decreases as the temperature of the contact parts increases, and thermal cracks due to recursive temperature changes may form, affecting the safety of the vehicle. Therefore, it is very important to release the frictional heat to the atmosphere effectively. Disc brakes are used in almost all automobiles and industrial machines, so their cooling performance is more important than that of other braking devices.

Helically fluted grooves have been introduced on the inner surfaces of circular tubes to enhance their heat transfer rates by increasing their surface area for heat convection, as well as providing for more active mixing of the surrounding fluid. Baughn and Yan [2], Han et al. [3], and Ravigururajan and Bergles [4] have investigated the shape of such grooves. Cho et al. [5, 6] studied the local heat transfer of various rib arrangements and determined that the heat transfer rate from a rectangular duct with a rib installed on its surface was 1.5-2.0 times that of a duct with no ribs. Yampolsky et al. [7] and Panchal et al. [8] conducted a heat transfer experiment with spirally fluted tubes and reported that the heat transfer rate was enhanced by 50-200% over that of a smooth tube. Obot et al. [9] determined that the friction factor of a spirally fluted tube was generally greater than that of a smooth tube in the laminar, transitional, and turbulent flow regimes. Lijun et al. [10] showed that the total heat transfer coefficient of a vertical tube was 63 ~ 95% greater than that of a smooth tube, with only a slight increase in the friction coefficient. Field results demonstrated the total heat transfer coefficient of a high-pressure preheater with tubes was increased 43%. However, because of the complex three-dimensional shapes involved, only the average heat transfer was measured in these studies.

Based on the research of Moon et al. [11], Syred et al. [12] proved that the heat transfer rate doubled when there was a dimple on a flat surface. As a result, semi-circular grooved fins have been placed on flat plates to enhance the heat transfer rate. Mahmood and Ligrani [13] investigated the heat transfer from a dimpled channel, including the combined influences of aspect ratio, temperature ratio, Reynolds number, and flow structure. The heat transfer rate with the groove increased to a maximum of 92.8% over that of a flat plate.

In this study, the hydrodynamically fully developed flow entered a circular tube with helically fluted grooves. The angle of the flute was fixed at 45° to study the variation in the heat transfer with the Reynolds number and distance from the entrance of the tube. The dimensionless streamwise distance (z/d) ranged between 1.5 and 4.5, and the Reynolds number varied from 30,000 to 70,000. The local heat transfer coefficients from the windward crest to the leeward crest of the helical flute were measured by using thermochromic liquid crystals and a digital color image-processing system. It is worth noting that when the liquid crystal/shroud-transient technique is utilized, local heat transfer coefficients can be accurately measured in complex three-dimensional shapes like ours.

2. Experimental apparatus and procedure

Fig. 1 shows a schematic diagram of the experimental apparatus used for this study. First, a centrifugal fan blew laboratory air through a copper tube. The fan speed was controlled by an inverter and the air flow rate was measured with an ASME orifice flow meter and a micro-manometer (MERIAM/34 MB 2 TMs) to an accuracy of ± 0.001 cm (water column). The air temperature was maintained to within ± 0.2 °C by way of the heat exchanger through which water from a constant temperature water bath was circulated. The copper tube was then connected to an acrylic tube having an inner diameter (d) of 7 cm and a length (z) of 245 cm. A bundle of straws were inserted inside the acrylic tube as flow straighteners to increase the dimensionless streamwise distance (z/d), so that a hydrodynamically fully developed flow entered the test section which was connected downstream from the acrylic tube. K-type (Chromega-Alumega) thermocouples were used to measure temperatures of the fluid and the test section. These were connected to a data acquisition system (OMEGA/DATA Shuttle 12-bit A/D board and Pentium Computer) and calibrated against a platinum-resistance thermometer in a constant temperature water bath (NESLAB/RTE-221D).

Figs. 2 and 3 show schematic diagrams of the shroud-transient method and the test model, respectively. Helically fluted grooves were installed inside a cast Nylon (MC801) circular tube. The top half of the acrylic tube was transparent (see Fig. 4), providing a

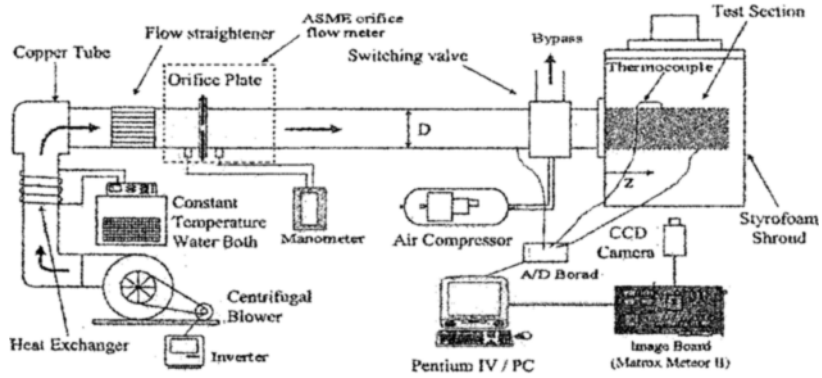

Fig. 1. Schematic diagram of the experimental apparatus.

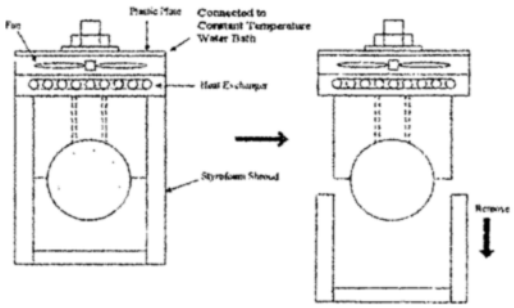

Fig. 2. Schematic diagram of the shroud-transient technique.

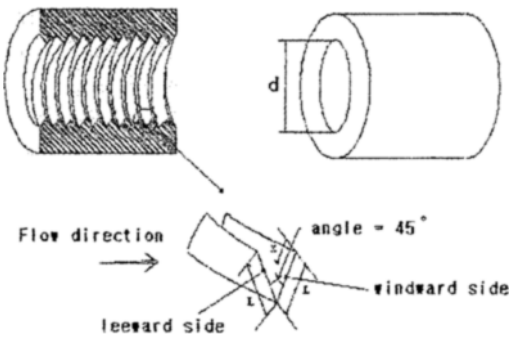

Fig. 3. Schematic diagram of the test model.

window to observe color changes of the liquid crystal. The bottom half of the cast Nylon tube surface was coated with black paint and liquid crystals by using an air brush. The test model was then placed inside the constant temperature air oven called, the shroud, which was fabricated from 5-cm-thick Styrofoam insulation sheets. A fan and heat exchanger were installed in the upper part of the shroud. Water from the constant temperature bath circulated through the heat exchanger, exchanging the energy with the air

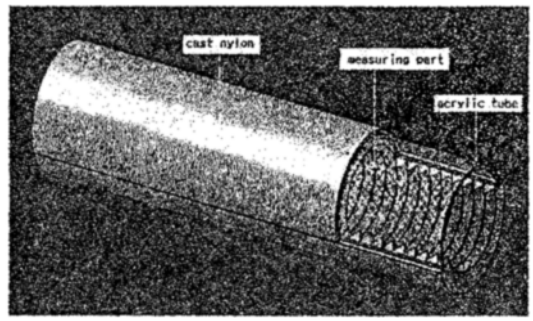

Fig. 4. Schematic view of the liquid crystal measuring window.

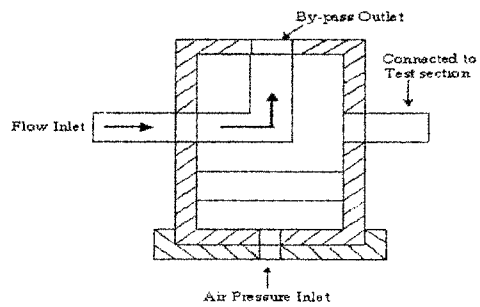

(a) Switching valve in by-pass position

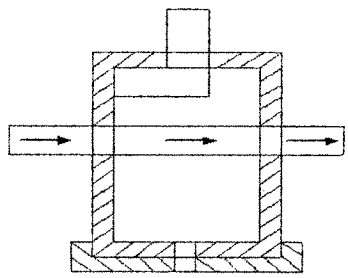

(b) Switching valve in run position

Fig. 5. Schematic diagram of the switching valve.

supplied by the fan. The air then heated the model uniformly to a temperature about 8 to 10 °C above the temperature at which red color of the liquid crystal began to appear. The model was heated inside the shroud until the maximum temperature difference along the body became less than ± 0.2 °C.

The flow switching bypass valve is illustrated in Fig. 5. When the test model reached a desired temperature and remained at steady-state, cooling air was allowed to enter the model and the shroud was suddenly removed by way of the switching valve for $1/30^{th}$ of a second. The switching valve was operated by high-pressure air supplied by an air compressor when a solenoid valve was opened, allowing the fluid to pass through and cool the model. The color of liquid crystal coated on the surface of the model began to change to red where the heat transfer rate was greatest. Then, the time-dependent heat transfer coefficient was measured on both the windward and leeward sides of the helical flute, by using a digital color image processing system (see Fig. 3).

3. Experimental analysis

The principle of the liquid crystal/transient technique is to calculate the local heat transfer coefficient by using a temperature difference between surface and ambient fluid, and an elapsed time for this difference to occur. A one-dimensional heat conduction approximation is used since the surface temperature response is limited to a thin layer near the surface and lateral conduction can be shown to be small (Baughn and Yan [2]). Therefore, one-dimensional conduction into a semi-infinite medium with a convective boundary condition is assumed and it has the following solution:

$$T^* = \frac{T_{LC} - T_j}{T_i - T_j} = e^{\lambda^2} erfc(\lambda) \tag{1}$$

Where T_{LC} is the surface temperature determined by liquid crystal, T_j is the inlet fluid temperature, T_i is the initial surface temperature, and erfc(γ) is the complementary error function, respectively. In Equation (1)

$$\lambda = \frac{(h_c + h_r)\sqrt{t}}{\sqrt{\rho Ck}} \tag{2}$$

Now, the convection heat transfer coefficient h_c is calculated as

$$h_c = \frac{\lambda\sqrt{\rho Ck}}{\sqrt{t}} - h_r \tag{3}$$

Where t represents the time for the surface temperature difference $(T_i - T_{LC})$ to occur, h_r is the radiation heat transfer coefficient $(= \varepsilon\sigma(T_{ref} + T_j)(T_{ref}^2 + T_j^2))$, ε is the emissivity of the liquid crystal/black paint coated surface, and T_{ref} is the average surface temperature $(= 0.5(T_i + T_{LC}))$.

The Nusselt number can be determined as follows:

$$Nu = \frac{h_c d}{k_a} \tag{4}$$

An uncertainty analysis was performed by using the method suggested by Kline and McKlintock [14]. It is shown in Table 1 that the Nusselt number uncertainty for z/d = 4.5 and $0 \le x/2L \le 1$ at Re = 50,000 is 4.68%. The uncertainty in the property of the cast Nylon is the largest contribution to the overall uncertainty and the uncertainty of the surface temperature measured by the liquid crystal is the second largest contribution.

4.1 Discussion of experimental results

Figs. 6-8 show the local Nusselt number distributions along the length of the helical flute for three Reynolds numbers of Re = 30,000, 50,000, 70,000 at three dimensionless streamwise distances of z/d = 1.5, 3.0, 4.5, respectively. In these figures the distance between the flute crest and valley is L = 10 mm. And x/2L = 0 and x/2L = 1 correspond to the windward crest and leeward crest, respectively, while x / 2L = 0.5 corresponds to the valley. It is shown from all

Table 1. Nusselt number uncertainty analysis.

X_i	*value*	δX_i	$\left(\frac{\delta X_i}{Nu}\frac{\partial Nu}{\partial X_i}\right)\times 100(\%)$
$\sqrt{\rho Ck}$	1085.98	44.83	3.84
T_{LC}	34.83	0.25	2.89
T_i	40.2	0.15	1.90
T_j	24.46	0.15	0.59
d	0.07	0.00005	0.23
t	658.97	0.03	0.2
Total Nu uncertainty			$\delta Nu / Nu = 4.68\%$

figures that the Nusselt number increases with the Reynolds number, and the largest Nusselt numbers appear to occur at the crest with their magnitudes being larger in the windward side than in the leeward side. This behavior is attributed to the flow impingement on the windward side. In the meantime the Nusselt number sharply decreases as the valley of the flute is approached from the crest because the fluting-guided fluid flow tends to recirculate and reside near the valley, resulting in the heat transfer reduction. It should be noted that we were not able to obtain the local Nusselt numbers very close to both the crest and the valley due to some measurement difficulties in those regions.

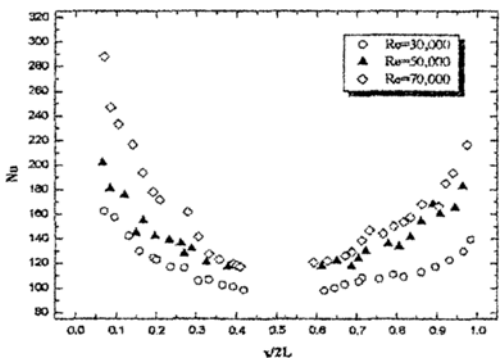

Fig. 6. istributions of the local Nusselt number for z / d = 1.5.

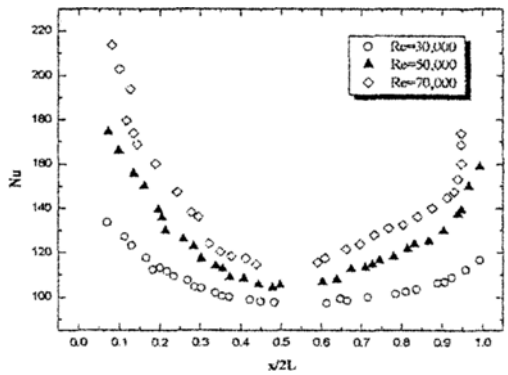

Fig. 7. Distributions of the local Nusselt number for z / d = 3.0.

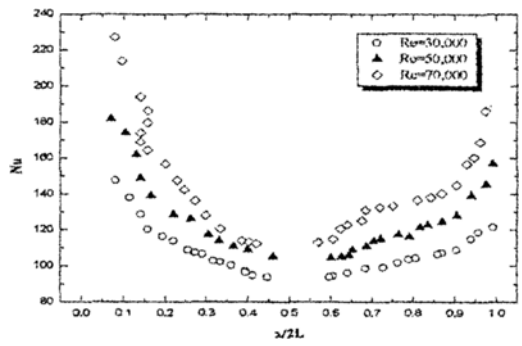

Fig. 8. Distributions of the local Nusselt number for z / d = 4.5.

It is shown from Figs. 7 and 8 that a trend of the Nusselt number distributions at z/d = 3.0 is very similar to that at z/d = 4.5, indicating that both hydrodynamic boundary layer and thermal boundary layer at and beyond z/d = 3.0 are fully developed. This trend is more pronounced in the leeward side than in the windward side according to Figs. 9~11, which will be explained in more detail shortly.

Figs. 9-11 are the same local Nusselt distributions as shown in Figs. 6-8, but differently plotted in order to investigate how the dimensionless streamwise distance (z/d) and length of the helical flute (x/2L) affect the local Nusselt number for Reynolds numbers of 30,000, 50,000, and 70,000. They clearly demonstrate very similar behaviors in the Nusselt number distributions for all Reynolds numbers at z/d = 3.0 and 4.5 with an exception in the windward crest region corresponding to $0.07 \leq x/2L \leq 0.15$. It appears that the Nusselt number magnitudes in the region ($0.07 \leq x/2L \leq 0.15$) at z/d = 4.5 are maximum 10 % larger than those at z/d = 3.0, maybe suggesting that the fluting-induced swirl motion carries away further downstream beyond z/d = 3.0, impinges near the windward crest region, and causes a more active mixing, resulting in heat transfer augmentation. This behavior is more pronounced as the Reynolds number decreases. It is also seen from Figs. 9-11 that as z/d increases, the shape of the Nusselt number distributions between in the windward and leeward sides of the flute is becoming more symmetric.

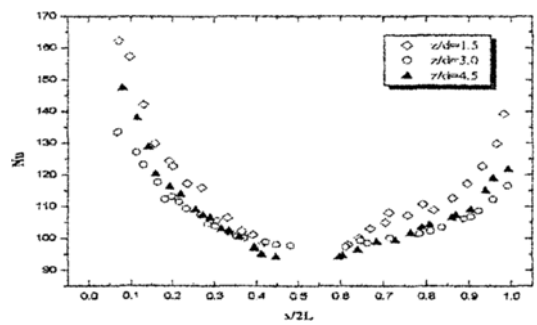

Fig. 9. Distributions of the local Nusselt number for Re = 30,000.

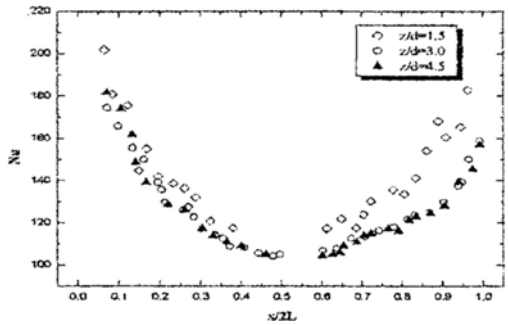

Fig. 10. Distributions of the local Nusselt number for Re = 50,000.

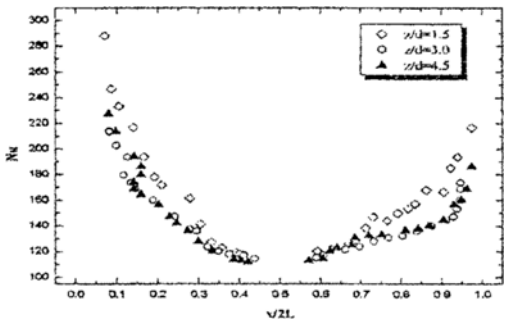

Fig. 11. Distributions of the local Nusselt number for Re = 70,000.

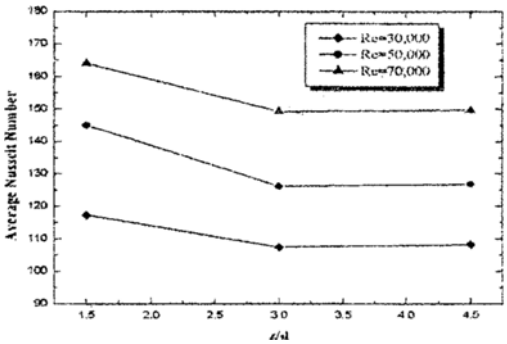

Fig. 12. Average Nusselt number distributions with z/d for different Reynolds numbers.

Fig. 12 shows the average Nusselt number distributions over $0 \le x/2L \le 1.0$ for different Reynolds numbers and z/d's. The average Nusselt number increases with the Reynolds number. For all Reynolds numbers, the average Nusselt number rapidly decreases for $1.5 \le z/d \le 3.0$ and remains the same for $z/d > 3.0$. This is because $1.5 \le z/d \le 3.0$ corresponds to a region of hydrodynamically, but not thermally, fully developed flow. The average Nusselt numbers, both

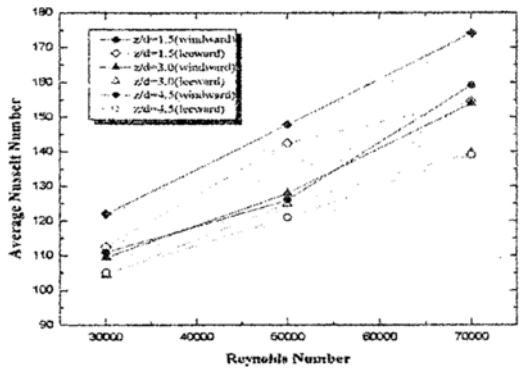

Fig. 13. Average Nusselt number distributions with Reynolds numbers in windward and leeward sides for different z/d.

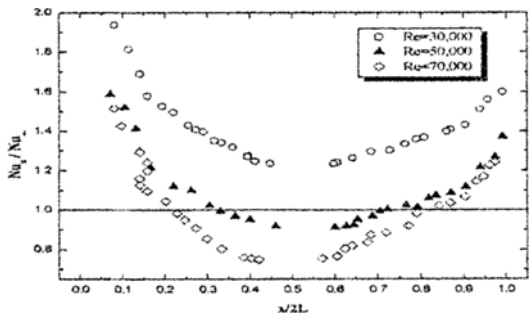

Fig. 14. Nusselt numbers normalized by the fully developed values at z / d = 4.5.

in the windward side and in the leeward side for different Reynolds numbers and z/d's, are shown in Fig. 13. The average Nusselt number in the windward side is 11.2 % higher than that in the leeward side. The smallest difference occurs for Re = 50,000, while the largest difference occurs for Re = 70,000.

In order to show the heat transfer augmentation in the helically fluted tube, the local Nusselt numbers at z/d = 4.5 and three Reynolds numbers of Re = 30,000, 50,000, 70,000 were normalized by the fully developed Nusselt numbers in the smooth tube and are shown in Fig. 14. The local Nusselt number data at z/d = 4.5 are chosen because both the velocity boundary layer and thermal boundary layer are believed to be fully developed. The fully developed Nusselt numbers in the smooth tube are obtained from the equation $Nu = 0.023\ Re^{0.8}\ Pr^{0.4}$ presented by Dittus and Boelter [15]. The results show that the local Nusselt numbers in the helically fluted tube are maximum 51.6 to 93.7 % higher than those in the smooth tube, and the average Nusselt number increases by 37 % when Re = 30,000 due to the increased surface area

provided by the helical fluted geometry, as well as the enhanced mixing of the fluid due to flow recirculation and swirl.

Fig. 14 also shows that as the Reynolds number increases, its rate of increase decreases. In fact, the heat transfer rates in some region along the flute at Re = 50,000 and 70,000 are smaller than those in a smooth tube because the flute is too deep. This phenomenon occurs when the depth of one side exceeds 6 mm (x/2L = 0.3 and 0.7) for Re = 50,000, and 4 mm (x/2L = 0.2 and 0.8) for Re = 70,000. This behavior may be attributed to the fact that as the Reynolds number increases, the flow rate also increases and secondary flow patterns are becoming stronger. However, the secondary flow vortices formed near the surface of the helical flute begin to disappear as the Reynolds number continues to increase. Therefore, it follows that in the deep helical flute, the momentum reduction of the fluid flow is more dominant than the heat transfer enhancement caused by flow separation and recirculation.

4.2 Discussion of numerical analysis and results

Fig. 15 shows a schematic diagram of the ventilated disc brake with helically fluted surface that has been proposed to enhance the heat dissipation in the cooling passage of the disc brake. In order to examine the thermal characteristics in the disc brake with helically fluted surfaces, 3-D finite element method was carried out. Fig.16 shows the finite element model of the ventilated disc brake. The number of vent holes (cooling flow passages in the disc brake) in the numerical model is the same as a commercial disc brake having 32 holes. 3-D FEM analysis using ANSYS has been carried out using only 1/64th of the ventilated disc brake with 11.25 degree interval and a geometrical symmetry. The mesh of each model was divided into the same scale.

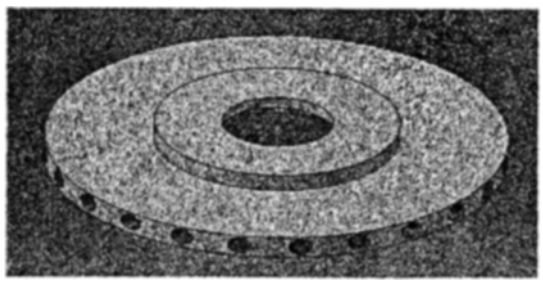

Fig. 15. Schematic view of the ventilated disc brake.

As a vehicle slows down using the brakes, kinematic energy converts to other energy due to not only the friction between the pad and the disc, but also the friction between the wheel and the land surface and the loss by air drag. However, it is assumed according to Lee et al. [16] that all kinematic energy converts to the frictional energy between the pad and the disc. Therefore, the heat flux due to the frictional energy can be obtained by the following equation:

$$q = \frac{a\gamma(m + \frac{I}{r^2})[2V_1 - a(t_2 - t_1)]}{10\pi(R_o^2 - R_i^2)} \tag{5}$$

where I is the inertia moment of the wheel, V_1 is the initial velocity of the vehicle, a is the ratio of the acceleration to the deceleration of the vehicle, r is the radius of the tire, R_o is the outside radius of the pad, R_i is the inside radius of the pad and m is the mass of the vehicle, and heat distribution ratio, γ is expressed as :

$$\gamma = \frac{q_d}{q_d + q_v} = \frac{1}{1 + \left(\frac{\rho_p c_p k_p}{\rho_d c_d k_d}\right)} \tag{6}$$

where ρ is the density, c is the specific heat, k is the thermal conductivity, subscripts d and p represent the disc and the pad, respectively.

Fig. 17 shows a variation of the vehicle speed with time under the braking condition. It was calculated on the basis of the condition that a vehicle moving with a speed of 90 km/h decelerates and accelerates repeatedly. This calculation result has been used as the input condition in the numerical analysis. The material properties for the disc brake are listed in Table. 2. The local heat transfer coefficients along the vent hole were experimentally obtained. And for more realistic

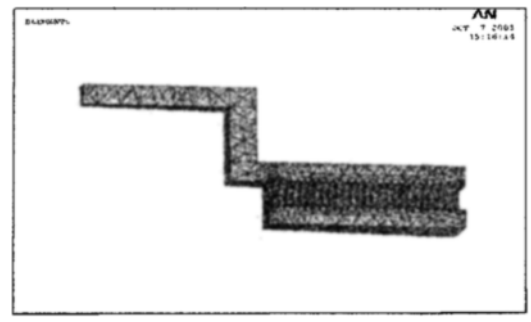

Fig. 16. Finite element model of the ventilated disc brake.

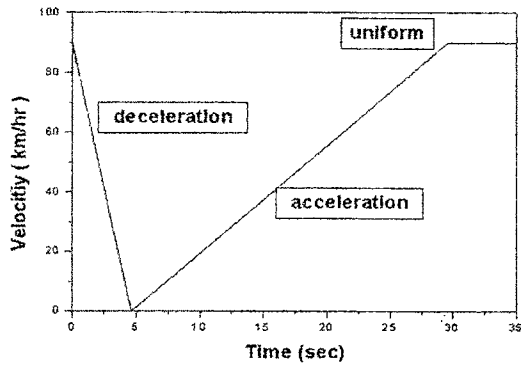

Fig. 17. A variation of vehicle speed under the braking condition.

Table 2. Material properties for the disc brake.

Material properties	Values
Elastic modulus, MPa	1.25×10^5
Poisson's ratio	0.25
Mass density, kg/m^3	7100
Coefficient of thermal expansion, 1/deg K	12×10^{-6}
Thermal conductivity, W/m·K	54
Specific heat, J/kg·K	586

FEM analysis to accurately determine the temperature distribution along the vent hole, the local value of heat transfer coefficient was used. In the past due to a difficulty in obtaining the local heat transfer coefficient inside the vent hole, only the average heat transfer coefficient obtained from the known correlation was used for the numerical analysis.

Figs. 18-20 show the temperature distributions along the vent hole surface with 10 cycles braking (35 seconds per each cycle). It is observed in general that the case with helically fluted surface has higher heat transfer coefficient than that with flat surface, resulting in the lower temperature distributions along the vent hole surface.

Compared with the flat surface case with 10 cycles braking, the temperature distributions with helically fluted surface are maximum 44.3 %, 36.8 %, and 36.6 % lower in the inlet, the center, the outlet, respectively. The maximum temperature difference in the entire vent hole is 55.5 °C with flat surface, but only 40.7 °C with helically fluted surface, achieving a more uniform temperature distribution with lower surface temperature. Therefore, it is expected that thermal cracks, hot spots, and the change of material

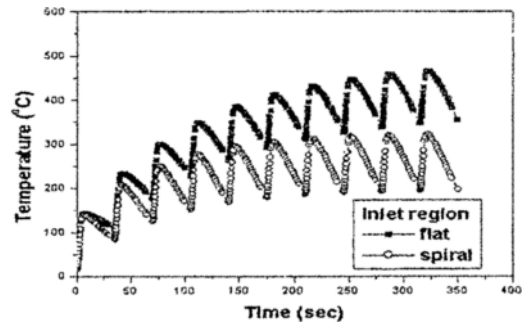

Fig. 18. Temperature distribution at the inlet of vent hole.

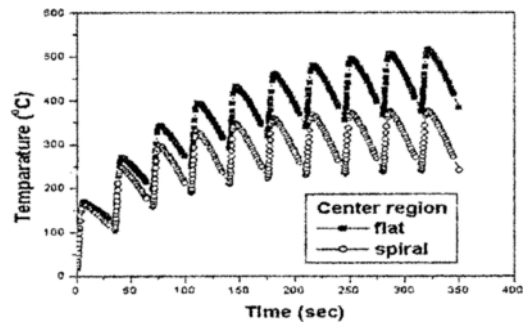

Fig. 19. Temperature distribution at the center of vent hole.

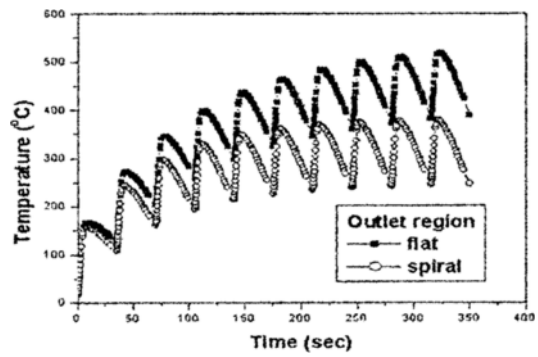

Fig. 20. Temperature distribution at the outlet of vent hole.

properties of the disc brake are less likely to occur with a helically fluted surface than with a flat surface.

5. Conclusions

In the present study, in order to enhance the heat transfer rate in the ventilated disc brake, the surface geometry in the flow passage of the disc brake has been modified from smooth surface to helically fluted surface. The main conclusions of local heat transfer measurements and numerical analysis are as follows.

(1) In general, the local Nusselt numbers mono-

tonically decrease with a distance away from both windward and leeward crests of the helical flute and reach a minimum value near its valley for all Re's and z/d's tested.

(2) The local Nusselt numbers on the helically fluted grooves are maximum 51.6 to 93.7 % higher than values measured on the smooth surface. This enhancement is attributed to the increased surface area provided by the helical fluted geometry, as well as the enhanced mixing of the fluid due to flow recirculation and swirl. The magnitudes of heat transfer enhancement become more pronounced with smaller Re and z/d.

(3) The largest enhancement occurs at the windward side of the helical flute at z/d = 1.5 and Re = 30,000. It is also found that at Re=30,000 the average Nusselt numbers on the helically fluted surface are maximum 37 % higher than those on the smooth surface.

(4) For Reynolds numbers higher than Re = 30,000, when the helical flute is too deep, the heat transfer rate is decreased. This occurs when the depth of one side exceeds 6 mm (x/2L=0.3 and 0.7) at Re = 50,000 and 4 mm (x/2L=0.2 and 0.8) at Re = 70,000.

(5) Compared with the smooth surface case when 10 cycles braking, the temperatures with helically fluted surface are maximum 44.3 %, 36.8 %, 36.6 % lower in the inlet, the center, the outlet, respectively.

Acknowledgment

This work was supported by the Inje Research and Scholarship Foundation in 2005.

Nomenclature

a : Ratio of acceleration to deceleration of the vehicle
C : Specific heat of Nylon (J/kg·K)
d : Diameter of the helically fluted tube (m)
h_c : Convection heat transfer coefficient(W/m^2·℃)
I : Moment of inertia of the wheel (N·m)
k : Thermal conductiviey of Nylon (W/m·K)
k_a : Thermal conductivity of the air (W/m·K)
k_d : Thermal conductivity of disc brake (W/m·K)
k_p : Thermal conductivity of disc pad (W/m·K)
L : Length from crest to valley of the helical flute (m)
m : Mass of the vehicle (kg)
Nu : Local Nusselt number ($= hd/k_a$)
r : Radius of the tire (m)
Re : Reynolds number ($=V_a \cdot d/\nu$)
R_o : Outside radius of the pad (m)
R_i : Inside radius of the pad (m)
T_j : Inlet fluid temperature (℃)
T_i : Initial temperature of the helically fluted tube (℃)
T_{LC} : Wall temperature measured by the color of liquid crystal (℃)
V_a : Velocity of the air (m/s)
V_l : Initial velocity of the vehicle (m/s)
z/d : Dimensionless streamwise distance
z : Length of the acryl tube (m)

Greek symbols

γ : Heat distribution ratio
ρ_d : Density of the disc brake (kg/m^3)
ρ_p : Density of the disk pad (kg/m^3)
ν : Kinematic viscosity of air (m^2/s)

References

[1] A. J. Day and A. B. Ashi, Heat flow and temperatures in friction material during braking, Proceedings of Institute of Mechanical Engineering, (1991).

[2] J. W. Baughn and X. Yan, A heated wall transient method for measurements of the heat transfer from a flat surface to a circular impinging jet, Proceedings of the Eurotherm Conference, (1991) 1-7.

[3] J. C. Han, Y. M. Zhang and C. P. Lee, Augmented heat transfer in square channels with parallel, crossed, and v-shaped angled ribs, *ASME Transactions*, 113 (1991) 590-596.

[4] T. S. Ravigururajan and A. E. Bergles, General correlations for pressure drop and heat transfer for single phase turbulent flow in internal ribbed tubes augmentation of heat transfer in energy systems, ASME-HTD, 52 (1985) 9-20.

[5] H. H. Cho, S. J. Wu and H. J. Kwon, Local heat/mass transfer measurements in a rectangular duct with discrete ribs, The 44th ASME Gas Turbine and Aeroengine Technical Congress, (1999).

[6] H. H. Cho, Y. W. Nam and D. H. Rhee, Local heat/mass transfer with various rib arrangement/effusion cooling system with crossflow," *Journal of Turbomachinery*, 126 (2004) 615-626.

[7] J. Yampolsky, P. A. Libby and B. E. Launder, Fluid mechanics and heat transfer in spirally fluted tubing, General Atomic Technology Report, GA-A17833,

(1984).

[8] C. B.Panchal, D. M. France and K. J. Bell, Experimental investigation of single-phase, condensation and flow boiling heat transfer for a spirally fluted tube, *Heat Transfer Engineering*, 1 (1992) 42-52.

[9] N. T. Obot, E. B. Esen and K. H. Snell, Pressure drop and heat transfer characteristics for air flow through spirally fluted tubes, ASME-HTD, 164 (1991) 85-92.

[10] W. Lijun, S. Da-Wen, L. Ping, Z. Lixian and T. Yingke, Experimental studies on heat transfer enhancement of the inside and outside spirally triangle finned tube with small spiral angles for high-pressure preheaters, *International Journal of Energy Research*, 124 (2000) 309-320.

[11] H. K. Moon, T. O'Connell and T. Glezer, Channel height effect on heat transfer and friction in a dimpled passage, International Gas Turbine and Aeroengine Congress Paper, No. 1999-GT-169, (1999).

[12] N. Syred, A. Khalatov and A. Kozlov, Effect of surface curvature on heat transfer and hydrodynamics within a single hemispherical dimple, International Gas Turbine and Aeroengine Congress, No. 2000-GT-236, (2000).

[13] G. I. Mahmood and P. M. Ligrani, Heat transfer in a dimpled channel: combined influences of aspect ratio, temperature ratio, Reynolds number, and flow structure, *International Journal of Heat and Mass Transfer*, 45 (2000) 2011-2020.

[14] S. J. Kline and F. A. McKlintock, Describing uncertainties in single sample experiments, *Mechanical Engineering*, 75 (1953) 3-8.

[15] F. W. Dittus and L. M. K. Boelter, Univ. of California (Berkeley) Pub. Eng., 443(2) (1930).

[16] S. K. Lee, B. Y. Sung and S. K. Ha, Optimal design of ventilated disc brake rotor, *Trans. of KSME (A)*, 24(3) (2000) 593-602.